Progress In Electromagnetics Research C, Vol. 19, 47–59, 2011

THE EFFECT OF ELECTRODE MATERIALS ON THE OPTICAL CHARACTERISTICS OF INFRARED QUANTUM DOT-LIGHT EMITTING DEVICES

A. E. Farghal, S. Wageh, and A. A. El-Azm

Faculty of Electronic Engineering
Menufiya University, Menouf 32952, Egypt

Abstract—We present an optical model based on Green's function to investigate the effect of using Single Wall Carbon Nanotube (SWCNT) as anode for infrared quantum dot light emitting devices (IR QD-LEDs). To the best of our knowledge there is no report in using SWCNT as anode in IR QD-LEDs. We have studied the emitted power distribution among the different optical modes (air, substrate, anode/organics, and surface plasmon modes (SP)), angular intensity distribution, and the emission spectral characteristics. We have found that the light outcoupling efficiency of IR QD-LEDs based on SWCNT as anode was increased nearly by a factor of 4 relative to that one based on indium-tin oxide (ITO). We also investigated the effect of using different cathode materials on the optical characteristics of IR QD-LEDs.

1. INTRODUCTION

Indium-tin oxide (ITO) has been dominantly used as transparent electrode for decades in flat panel displays, solar cells, organic light emitting diodes (OLED), and Quantum dot organic light emitting diodes (QD-LED), due to its excellent transparency and relatively high conductivity. ITO is a highly degenerate n-type semiconductor with a wide band gap semiconductor (E_g: 3.5–4.7 eV) [1, 2], and has a low electrical resistivity of $2-4\times10^{-4}\,\Omega\cdot$cm. ITO shows good transmission in the visible and near-infrared (NIR) regions of the electromagnetic spectrum. Furthermore, ITO also has shown good efficiency for hole injection into organic materials.

Received 26 November 2010, Accepted 29 December 2010, Scheduled 10 January 2011
Corresponding author: Ahmed E. Farghal (ahmedfarghal7080@gmail.com).

However, ITO has several limitations for current and future generation LEDs. It has limited chemical stability leading to diffusion of oxygen into proximate organic layers, relatively low work functions ($\sim 4.7\,\text{eV}$), also, its increasingly expensive due to the limited worldwide production of indium which may soon find difficulty meeting the ever increasing demand for large-scale transparent conductive electrodes [2, 3]. ITO is relatively brittle, which degrades its performance on flexible substrates [4]. Strong free-carrier absorption of infrared (IR) photons, which limits the device photo generated current in thin film photovoltaic (PV) devices [5]. Also, ITO shows high reflectivity in the IR region [6], and only transmits 70% at 1500 nm [7].

New transparent electrodes are needed in QD-LED to provide higher transmittance in the IR portions of the spectrum. In response to these limitations, SWCNTs have received increasing attention as ITO alternatives [2, 4].

The SWCNT networks have a work function in the 4.7–5.2 eV range. Such high work function meets the requirement for anodes in several types of optoelectronic devices, such as OLED and organic solar cells. In addition, the nanotube films have large surface area due to the nanoporous structure which offer a potential for hole injection. Also, exceptional mechanical flexibility of SWCNT, the nanotube was repeatably deformable over 100% strain without causing a substantial change in conductance. Ordinary conductors cannot undergo nearly such large strains without losing electrical contact with the actuating material [2, 8].

On the other hand, SWCNT film fabrication on a flexible substrate is relatively simple, while ITO deposition on flexible substrates requires vacuum and elaborate process equipment [2, 3].

The SWCNT-based electrodes are highly conductive in thin layers, and optical measurements indicate superior optical transmission ($>$ 80%) in the IR (wavelengths $>$ 1200 nm) compared to traditional ITO, in addition to the absence of free-carrier absorption in that region [5]. These characteristic of SWCNT layer is a significant qualitative difference as compared to ITO. The SWCNT-based transparent electrodes have already been used in photovoltaic and OLEDs [2, 3, 5, 9]. However, to the best of our knowledge they have not been employed in IR QD-LEDs. Here we will study theoretically the effect of using SWCNT film as anode in comparison with ITO film on the optical characteristics of IR QD-LEDs.

The simulations presented in this work are based on the Poynting vector analytical expression developed by Celebi et al. [10] and followed our computations for the IR QD-LEDs [11]. Several other approaches for the simulation of OLEDs have been described in

the literatures; for example, the radiative transfer approach which allows one to compute only the color [12], Chance et al. [13] model which enables one to compute accurately the intensity, but only for simple device structures, Fermi's golden rule [14] which compute both the radiative and internal intensities, however, the validity of that approach is limited to lossless devices, and does not account for nonradiative losses to the metal electrodes or absorption, wave optics and transfer matrix formalism [15], but they cannot be directly applied to OLEDs, because OLED uses a thick glass substrate, which results in computational difficulty, and the scheme described by Kahen [14], is rigorous but not efficient, since the calculation involves the evaluation of the Sommerfeld-like integral which requires careful selection of the integration path, in addition, accurate computation of the far-field at a large viewing angle is inefficient due to the rapid oscillating nature of bessel function with the large argument. While the model presented here is straightforward model without numerical difficulties, and it takes into account the surface plasmon modes and absorption in different layers.

This article is organized as follows; the theoretical model is given in Section 2. The simulation results and the related discussion are presented in Section 3. Finally, conclusions are drawn in Section 4.

2. THEORY

he radiation field is described by constructing a Green's function for the multilayer medium containing the exciton and the total radiative energy is calculated by integrating the Poynting vector over the magnitude of the normalized in plane wavevector which varies from zero to infinite. Assuming that the QDs emitting layer contains the exciton radiators with random orientations, it can be decomposed into the vertical and horizontal exciton components. Therefore, we can compute the total radiation intensity by adding the vertical and horizontal exciton components. The vertical exciton power in each layer is given by [10]:

$$P_{z,j}^{V} = \Re\left(\int S_{z,j}^{V^*} dA\right) = \frac{3q}{4}\Re\left[\int_0^{\infty} du \frac{u^3(\sqrt{\varepsilon_j})^*}{|1-u^2|\sqrt{\varepsilon_j}}\sqrt{(\varepsilon_j/\varepsilon_5 - u^2)}\right.$$
$$\left.\left(R'_j e^{ih_j z} - R_j e^{-ih_j z}\right) * \left(R'_j e^{ih_j z} + R_j e^{-ih_j z}\right)\right] \quad (1)$$

and for an exciton oriented horizontal, the power is:

$$\begin{aligned} P_{z,j}^{H} &= \Re\left(\int S_{z,j}^{H^*}\, dA\right) \\ &= \frac{3q}{8}\Re\Bigg[\int_0^{\infty} du \frac{u(\sqrt{\varepsilon_j})^*}{\sqrt{\varepsilon_j}}\sqrt{(\varepsilon_j/\varepsilon_5 - u^2)}\left(R_j' e^{ih_j z} - R_j e^{-ih_j z}\right) \\ &\quad \left(R_j' e^{ih_j z} + R_j e^{-ih_j z}\right)^* + \int du \frac{u(\sqrt{(\varepsilon_j/\varepsilon_5 - u^2)})^*}{|1-u^2|} \\ &\quad \left(T_j' e^{ih_j z} + T_j e^{-ih_j z}\right)\left(T_j' e^{ih_j z} - T_j e^{-ih_j z}\right)^*\Bigg] \end{aligned} \tag{2}$$

where $P_{z,j}^{V}$, $P_{z,j}^{H}$ are the vertical and horizontal exciton power at each layer, respectively. S_z^V, S_z^H are the Poynting vectors in the Z direction for vertical and horizontal exciton, respectively. $h_j = \sqrt{k_j^2 - K^2}$, $K_j^2 = \varepsilon_j(\omega/c)^2$, h_j and K are the amplitudes of the horizontal and vertical components of the propagation vector, k. ε_j represents the complex dielectric constant, j is the layer index. ε_5 is the dielectric constant for QD layer (emission layer). $u = K/k_5$ is the normalized inplane wavevector at QD layer location. q is the intrinsic quantum yield of the QD emitting material. The coefficients T_j, R_j and T_j', R_j' correspond to the upward and downward traveling eigenfunctions, respectively which are founded by applying boundary conditions that the tangential electric fields are continuous across the interface between layers and the radiation conditions.

The exciton power transfer efficiency to an individual layer as a unitless percentage of the total power emitted is found by taking the difference of the magnitude of this flux found at both boundaries of the layer and then normalizing it to $\hat{b}_V$ or $\hat{b}_H$. Where $\hat{b}_V$ is the normalized decay rate for oscillating exciton oriented vertical in infinite medium, which is given by [16]:

$$\hat{b}_V = 1 - q + \frac{3}{2}q\left\{1 + \frac{3}{2}\Re\left[\int_0^{\infty} dK \frac{K^3}{h_5 K_5^3}(R_5 + R_5')\right]\right\} \tag{3}$$

and $\hat{b}_H$ is the normalized decay rate for oscillating exciton oriented horizontal in infinite medium, and given by:

$$\hat{b}_H = 1 - q + q\left\{1 + \frac{3}{4}\Re\left[\int_0^{\infty} dK \frac{K}{h_5 K_5}\left(T_5 + T_5' + \frac{h_5^2}{K_2^2}R_5 + R_5'\right)\right]\right\} \tag{4}$$

The fraction of the generated power can be divided into four different optical modes: direct transmission into the air mode, the glass total internal reflection mode, anode/organic waveguided mode, and plasmon mode in terms of the wavenumber k_o. Of this generated power, that fraction within the range $0 \leq K \leq 2\pi n_{air}/\lambda$ corresponds to the external modes of the QD-LED structures capable of producing useful far filed radiation.

In the case of plane waves propagating through multilayers, an emitting angle θ_{air} in the air region associated with K and wavevector $k_o = 2\pi n_{air}/\lambda$, according to the formula of $k_o \sin\theta_{air} = K$. The power in the K space can be transformed to a power in the real spatial space. The intensity angular distribution is related to the power P by

$$I(\theta_{air}) = \frac{P(K)}{2\pi \tan(\theta_{air})} \tag{5}$$

where $P(K)$ is $\frac{1}{3}P_{zj}^{V} + \frac{2}{3}P_{zj}^{H}$ for isotropic exciton power emitted in air as a function of K.

The device used in our calculation is depicted in Figure 1, and consists of a glass substrate, (160 nm) ITO anode (Figure 1(a))/ (160 nm) CNT anode (Figure 1(b)), (40 nm) 4,4-bis[*N*-(1-naphthyl)-*N*-phenyl-amino]biphenyl (α-NPD) as hole transporting organic layer, (20 nm) PbSe QD monolayer as emitting layer radiates typically at 1.5 µm, (40 nm), tris-(8-hydroxyquinoline) aluminum (Alq_3) as electron-transporting layer (ETL), and metal cathode (50 nm thick Mg/Ag, by weight, 50 nm Ag cap). Optical constants of Alq_3 and α-NPD are taken from [17], optical constants of ITO and Mg:Ag are taken from [18] and refractive index of SWCNT n, is taken the value of graphite [18, 19].

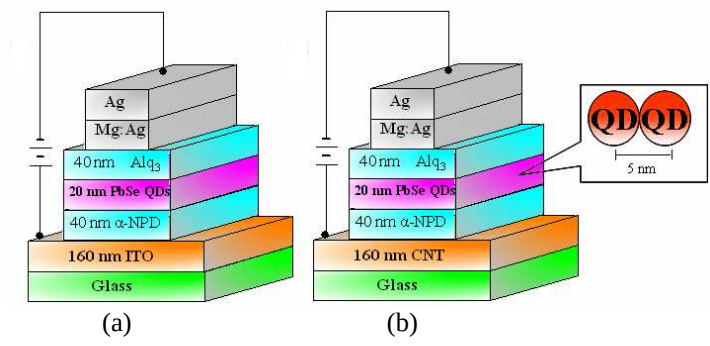

Figure 1. The schematic of the IR QD-LED device structure used in calculations for (a) ITO anode and (b) CNT anode.

3. RESULTS AND DISCUSSIONS

We have investigated the effect of changing the position of the emitting exciton within the emission QD layer on the coupling strength to different optical modes and on outcoupling efficiency of the device. We have computed the distribution of emitted IR radiation at 1.5 μm from QD-LED as a function of the exciton position within the emitting layer. Here we considered the emitting QDs packed regularly with 5 nm diameter and center-to-center distance equal 5 nm. In addition, we assumed that the exciton (emission point) lie in the middle of every QD.

Figures 2(a) and (b) and Table 1 show the distribution of light emission at 1.5 μm for glass/ITO/α-NPD/ PbSe QD/ Alq_3/ Mg:Ag/Ag QD-LED and glass/SWNT/ α-NPD/ PbSe QD/ Alq_3/ Mg:Ag/Ag QD-LED as a function of the exciton position within the QDs layer. The fraction of power that coupled in the anode layer for the two devices are largely dependent on the emitting center position within the emitting QD layer, and increases with increasing the distance from

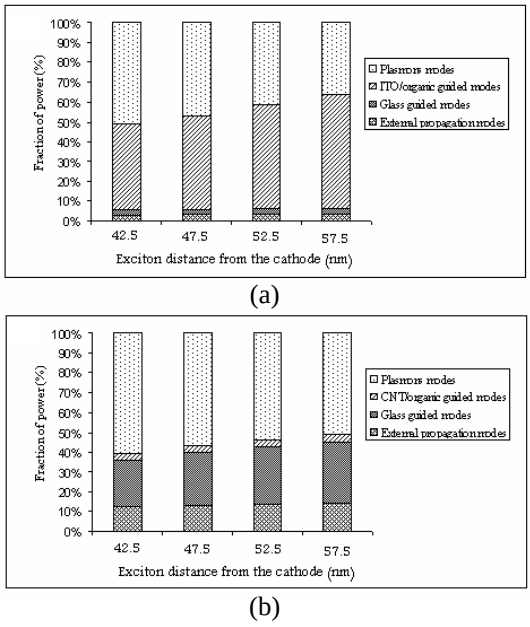

Figure 2. Calculated distribution of emission into the four optical modes versus the exciton distance from the cathode when (a) using ITO anode, (b) using SWCNT anode.

Table 1. Average calculated fractions of power emitted in each optical mode for ITO and CNT anodes.

	External modes (%)	**Glass guided modes (%)**	**Anode/organic guided modes (%)**	**Plasmon modes (%)**
ITO	3.341575	2.776425	49.8935	43.82875
CNT	13.34975	27.38375	3.695075	55.41625

the metal cathode. If the emitting exciton is close to the cathode, most of the power is coupled into SP modes. On the other hand, for the device based on SWCNT anode there is a significant increase in the eternal emission and decrease in the anode/organics modes as compared to the device based on ITO anode. The increase in these modes leads to increasing outcoupling efficiency. The outcoupling efficiency of the device based on SWCNT anode improved more than 3.99 times relative to the device based on ITO anode. We attributed the improvement in the outcoupling efficiency to the superior IR transmission of CNT compared to ITO [5], also the high refractive index of SWCNT ($n \sim 1.99$ at 1.5 µm) which lower the mismatch with high refractive index PbSe QD ($n \sim 4.6$) [20].

Figure 3 shows the angular radiation profile of isotropic exciton emission for glass/ITO/ α-NPD/ PbSe QD/ Alq_3/ Mg:Ag/Ag QD-LED and glass/SWNT/ α-NPD/ PbSe QD/ Alq_3/ Mg:Ag/Ag QD-LED. For the device based on ITO anode the angular radiation profile

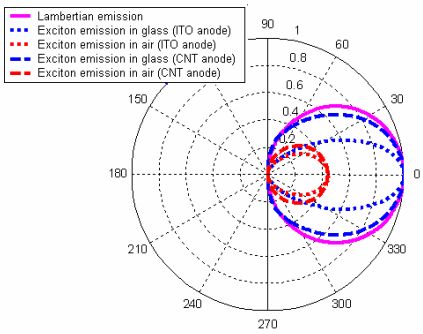

Figure 3. Radiation profiles of the isotropic exciton sources of NIR QD-LED structure at $\lambda = 1.5$ µm with CNT and ITO anode.

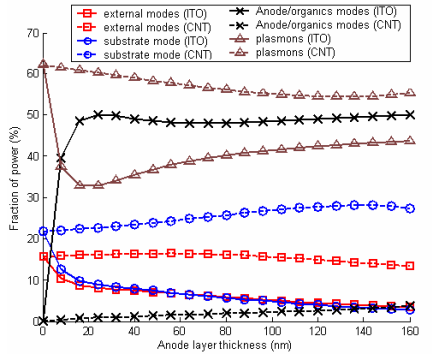

Figure 4. Simulation results of the power fraction coupled into the four optical modes with anode layer thickness variation for ITO and CNT anodes.

is not Lambertian and the light is stronger beaming in the forward direction which is consistent with the previously reported results for IR QD-LEDs [21, 22]. While for the device based on SWCNT anode the angular radiation profile is approximately Lambertian. We ascribed the non-Lambertian profile of the device based on ITO anode due to the large refractive index mismatch in the IR region between PbSe QD ($n \sim 4.6$) and ITO ($n \sim 0.5$). Also, the radiation intensity variation trend with anode type is consistent with the results in Table 1.

In Figure 4 we show the effect of varying the anode layer thickness on the fraction of exciton emitted power coupled into the four optical modes. Clearly, the external mode is less affected by anode thickness

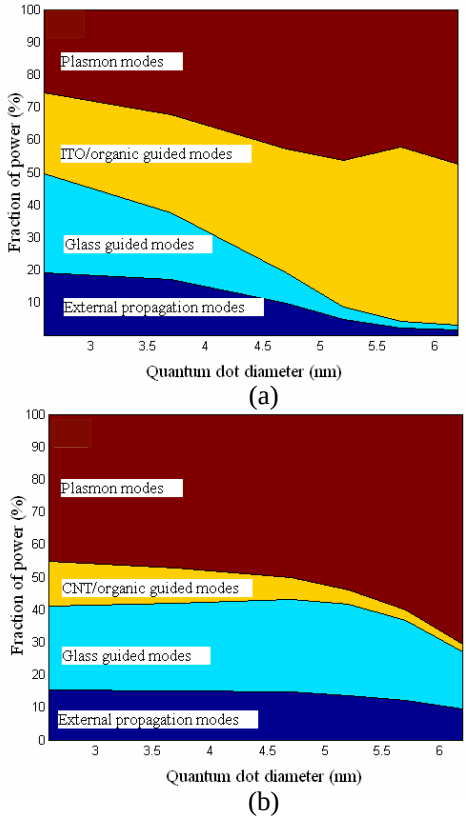

Figure 5. Simulation results of the power fraction coupled into the four optical modes as a function of QD diameter (nm) for (a) ITO anode, (b) SWCNT anode.

variation for the device based on SWCNT, but for the device based on ITO anode the fractional of external mode is decreased with increasing the anode thickness. We ascribed this result to constancy of the SWCNT transmission with thickness in IR region [3]. The anode/organics and SP modes are less affected by the variation of the SWCNT thickness. But for the device based on ITO anode the effect of anode thickness variation on the anode/organics and SP modes is only remembered at very low anode thickness. We should bear in mind; the thickness of anode layer of the device not only affects the optical characteristics but also affects the electrical characteristics.

Figures 5(a) and (b) show the variation in the fraction of the power coupled to the four optical modes as a function of QD diameter for the two devices based on ITO and SWCNT as anodes, respectively. Obviously, at smaller QD sizes the external emission is higher for the device based on ITO relative to that one based on SWCNT anode. Conversely, at larger QD sizes the external emission for the device based on SWCNT becomes superior relative to the device based on ITO anode. We attributed this result to the increase of transmission coefficient for the SWCNT and decrease of transmission coefficient for ITO at higher wavelengths. We also note that the anode/organic modes are greatly suppressed when using SWCNT as anode. Our computations also showed that a considerable amount of radiation is trapped inside the glass substrate and in the SP modes in the case of SWCNT, but the improvement in the external modes are significant.

Figure 6 shows the experimental measurements of the position of the first absorption peak versus the diameter of semiconductor

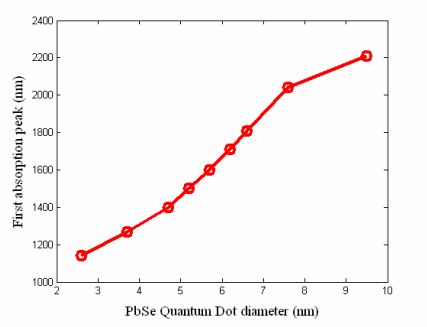

Figure 6. Diameter of semiconductor QDs versus the position of the first absorption peak. Data were taken from [7].

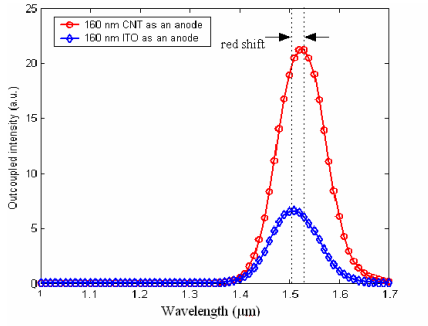

Figure 7. Calculated outcoupled emission spectra for IR-QDLED when using CNT and ITO anodes at $\lambda = 1.5\,\mu$m.

QD [7]. The figure demonstrates the wavelength tunability afforded by controlling the QD size (quantum confinement effect).

On other hand we have investigated the effect of replacing ITO anode by the SWCNT on the outcoupled emission intensity. The outcoupled emission intensity is calculated as in [11]. Figure 7 shows the calculated outcoupled emission spectra in the IR region for glass/ (160 nm) ITO/ (40 nm) α-NPD/(20 nm) PbSe QD/ (40 nm) Alq_3/ (50 nm) Mg:Ag/Ag and glass/ (160 nm) SWCNT/ (40 nm) α-NPD/ (20 nm) PbSe QD/(40 nm) Alq_3/ (50 nm) Mg:Ag/Ag devices. Clearly, the outcoupled power efficiency is significantly improved for the device based on the SWCNT anode more than 4 times relative to the device based on ITO anode. We also noted that there is a red-shift for the position of the emission peak when using SWCNT as anode instead of ITO anode.

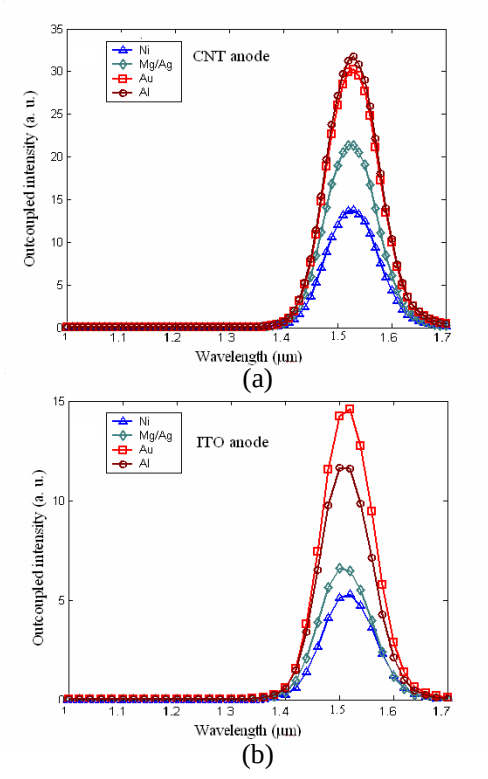

Figure 8. Simulation results of outcoupled power emission spectra at $\lambda = 1.5\,\mu$m with various cathode metals for the device based on (a) SWCNT anode, (b) ITO anode.

Figures 8(a) and (b) show the outcoupled emission intensity spectra for the glass/(160 nm) ITO/(40 nm) α-NPD/(20 nm) PbSe QD/ (40 nm) Alq_3/ (50 nm) different cathodes and glass/(160 nm) SWCNT/(40 nm) α-NPD/(20 nm) PbSe QD/(40 nm) Alq_3/ (50 nm) Mg:Ag/(50 nm) different cathodes, respectively. We have used Al, au, Mg/Ag and Ni for the cathode layer. The complex dielectric constants of these metals were obtained from [18]. We found that the outcoupled emission intensity is higher for Al and Au relative to Ni and Mg/Ag as cathode materials for the two devices. We attributed this result to the higher reflectivity of Al and Au relative to Ni and Mg/Ag cathodes. In general the outcoupled emission intensity for SWCNT-based devices with AL, Au, Mg/Ag and Ni cathode materials is higher than that for ITO-based devices with the same cathode materials. These results imply that a careful selection of cathode material will help in increasing the output intensity.

4. CONCLUSIONS

In conclusion, we have utilized a Green's function-based model to calculate the outcoupling efficiency of IR-QDLED using CNT anode. The calculations suggest that it is relatively simple to use CNT anode to increase the light outcoupling efficiency by a factor ~ 4. So, CNT is an ideal choice for IR-QDLEDs. Also we have investigated the effect of metal cathode material types on the optical characteristics of IR QD-LEDs. We have found that the application of Al and Au as cathode materials is better than Mg/Ag and Ni as cathode materials from optical characteristics point view point, especially in the case of SWCNT anode.

REFERENCES

1. Kima, H., C. M. G. A. Piqué, J. S. Horwitz, H. Mattoussi, H. Murata, Z. H. Kafafi, and D. B. Chrisey, "Electrical, optical, and structural properties of indium-tin-oxide thin films for organic light-emitting devices," *J. Appl. Phys.*, Vol. 86, No. 11, 6451–6461, 1999.
2. Li, J., L. Hu, L. Wang, Y. Zhou, G. Grüner, and T. J. Marks, "Organic light-emitting diodes having carbon nanotube anodes," *Nano Lett.*, Vol. 6, No. 11, 2472–2477, 2006.
3. Zhang, D., K. Ryu., X. Liu, E. Polikarpov, J. Ly, M. E. Tompson, and C. Zhou, "Transparent, conductive, and flexible carbon nanotube films and their application in organic light-emitting diodes," *Nano Lett.*, Vol. 6, No. 9, 1880–1886, 2006.

4. Green, A. A. and M. C. Hersam, "Colored semitransparent conductive coatings consisting of monodisperse metallic single-walled carbon nanotubes," *Nano Lett.*, Vol. 8, No. 5, 1417–1422, 2008.
5. Contreras, M., T. Barnes, J. van de Lagemaat, G. Rumbles, T. J. Coutts, C. Weeks, P. Glatkowski, I. Levitsky, and J. Peltola, "Application of single-wall carbon nanotubes as transparent electrodes in Cu (In, Ga) Se2-based solar cells," *IEEE Photovoltaic Energy Conversion Conference*, Waikoloa, Hawaii, 2006.
6. Kim, H., C. M. Gilmore, A. Piqué, J. S. Horwitz, H. Mattoussi, H. Murata, Z. H. Kafafi, and D. B. Chrisey, "Electrical, optical, and structural properties of indium-tin-oxide thin films for organic light-emitting devices," *J. Appl. Phys.*, Vol. 86, No. 11, 6451–6461, 1999.
7. Steckel, J. S., et al., "1.3 μm to 1.55 μm tunable electroluminescence from PbSe quantum dots embedded within an organic device," *Advanced Materials*, Vol. 15, No. 21, 1862–1866, 2003.
8. Zhang, M., S. F., A. A. Zakhidov, S. B. Lee, A. E. Aliev, C. D. Williams, K. R. Atkinson, and R. H. Baughman, "Strong, transparent, multifunctional, carbon nanotube sheets," *Science*, Vol. 309, No. 5738, 1215–1219, 2005.
9. Weeks, C., et al., "Single-wall carbon nanotubes as transparent electrodes for photovoltaics," *IEEE Photovoltaic Energy Conversion Conference*, Waikoloa, Hawaii, 2006.
10. Celebi, K., T. D. Heidel, and M. A. Baldo, "Simplified calculation of dipole energy transport in a multilayer stack using dyadic Green's functions," *Optics Express*, Vol. 15, No. 4, 1762–1772, 2007.
11. Farghal, A. E., S. Wageh, and A. E.-S. Abou-El-Azm, "Electromagnetic modeling of outcoupling efficiency and light emission in near-infrared quantum dot light emitting devices," *Progress In Electromagnetics Research B*, Vol. 24, 263–284, 2010.
12. Crawford, O. H., "Radiation from oscillating dipoles embedded in a layered system," *J. Chem. Phys.*, Vol. 89, No. 10, 6017, 1988.
13. Bulović, V., V. B. Khalfin, G. Gu, P. E. Burrows, D. Z. Garbuzov, and S. R. Forrest, "Weak microcavity effects in organic light-emitting devices," *Phys. Rev. B*, Vol. 58, No. 7, 3730, 1998.
14. Kahen, K. B., "Rigorous optical modeling of multilayer organic light-emitting diode devices," *Appl. Phys. Lett.*, Vol. 78, No. 12, 1649, 2001.

15. Chen, et al., "Electromagnetic modeling of organic light-emitting devices," *Journal of Lightwave Technology*, Vol. 24, No. 6, 2450, 2006.
16. Chance, R. R., A. Prock, and R. Silbey, "Molecular fluorescence and energy transfer near metal interfaces," *Advances in Chemical Physics*, I. Prigogine and S. A. Rice (eds.), 1–65, Wiley, 1978.
17. Himcinschi, C., N. Meyer, S. Hartmann, M. Gersdorff, M. Friedrich, H.-H. Johannes, W. Kowalsky, M. Schwambera, G. Strauch, M. Heuken, and D. R. T. Zahn, "Spectroscopic ellipsometric characterization of organic films obtained via organic vapor phase deposition," *Appl. Phys. A*, Vol. 80, No. 3, 551–555, 2005.
18. Palik, E. D., *Handbook of Optical Constants of Solids*, Academic, New York, 1985.
19. Wang, T., "Light scattering study on single wall carbon nanotube (SWNT) dispersions," Thesis, Georgia Institute of Technology, 2004.
20. Wehrenberg, B. L., C. Wang, and P. Guyot-Sionnest, "Interband and intraband optical studies of pbse colloidal quantum dots," *J. Phys. Chem. B*, Vol. 106, No. 41, 10634–10640, 2002.
21. Tessler, N., V. Medvedev, M. Kazes, S. H. Kan, and U. Banin, "Efficient near-infrared polymer nanocrystal light-emitting diodes," *Science*, Vol. 295, No. 5559, 1506–1508, 2002.
22. Bourdakos, K. N., D. M. Dissanayake, T. Lutz, S. R. Silva, and R. J. Curry, "Highly efficient near-infrared hybrid organic-inorganic nanocrystal electroluminescence device," *Appl. Phys. Lett.*, Vol. 92, No. 15, 153311, 2008.